Principles of self-assembly of helical pores from dendritic dipeptides

Virgil Percec*[†], Andrés E. Dulcey*, Mihai Peterca[‡], Monica Ilies*, Sami Nummelin*, Monika J. Sienkowska*, and Paul A. Heiney[‡]

*Roy and Diana Vagelos Laboratories, Department of Chemistry, University of Pennsylvania, Philadelphia, PA 19104-6323; and [‡]Department of Physics and Astronomy, University of Pennsylvania, Philadelphia, PA 19104-6396
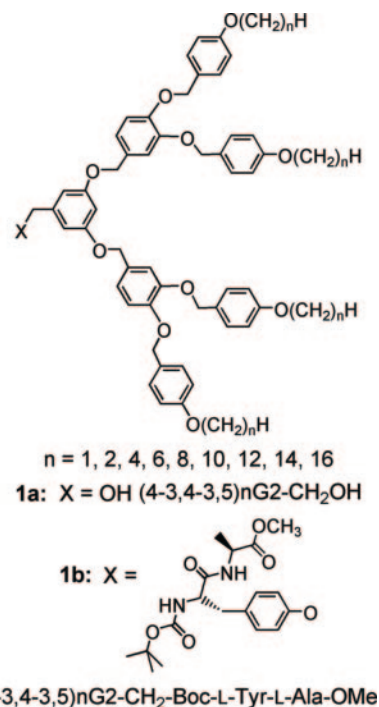
The self-assembly of the dendritic dipeptides (4-3,4-3,5)nG2-CH$_2$-Boc-L-Tyr-L-Ala-OMe and their achiral dendritic alcohol (4-3,4-3,5)nG2-CH$_2$OH precursors, both with $n = 1$–16, where n represents the number of methylenic units in the alkyl groups of the dendron, are reported. All chiral dendritic dipeptides and achiral dendritic alcohols self-assemble into helical porous columns that are stable in both solution and solid state. The pore diameter (D_{pore}) of the columns self-assembled from dendritic dipeptides is ≈10 Å larger than that of structures assembled from dendritic alcohols. The increase of the D_{pore} at the transition from dendritic alcohol to dendritic dipeptide is accompanied by a decreased solid angle of the building block. This trend is in agreement with previous pore size–solid angle dependences observed with different protective groups of the dipeptide and primary structures of the dendron. However, within the series of dendritic alcohols and dendritic dipeptides with various n, the D_{pore} increases when the solid angle increases. The results of these investigations together with those of previous studies on the role of dipeptide stereochemistry and protective groups on this self-assembly process provide the molecular principles required to program the construction of supramolecular helical pores with diameter controlled at the Å level from a single dendritic dipeptide architecture. These principles are expected to be valid for libraries of dendritic dipeptides based on dendrons and dipeptides with various primary structures.

chiral dendrons | porous supramolecular columns | protein mimics | peptide stereochemistry

Scheme 1. Structures of (4-3,4-3,5)nG2-CH$_2$OH (**1a**) and (4-3,4-3,5)nG2-CH$_2$-Boc-L-Tyr-L-Ala-OMe (**1b**).

Natural porous proteins function as viral helical coats (1), transmembrane channels (2, 3), antibiotics (4), and pathogens (5), and their remodeled structures are used in synthetic systems for reversible encapsulation (6) and stochastic sensing (7). With few exceptions (8–10) porous protein mimics do not assemble, as the natural porous proteins do, into periodically ordered structures that are stable in both solution and bulk (11–14). This behavior limits their structural analysis by combinations of solution and solid-state complementary techniques. Recently our laboratory (15) reported the self-assembly of amphiphilic dendritic dipeptides into helical porous structures that are stable in both solution and bulk (15). Preliminary reports have demonstrated that the internal structure and the stability of the porous columns self-assembled from dendritic dipeptides are programmed by the structure and stereochemistry of the dipeptide (15, 16), the protective groups of the dipeptide (17), and the structure of the dendron (18) attached to the dipeptide. Here we are reporting a comparative study of the self-assembly and structural and retrostructural analysis of the supramolecular porous structures generated from libraries of (4-3,4-3,5)nG2-CH$_2$-Boc-L-Tyr-L-Ala-OMe dendritic dipeptides and their achiral (4-3,4-3,5)nG2-CH$_2$OH precursors with $n = 1$–16. This series of experiments will provide the principles required to engineer at the molecular level biologically inspired functions via porous protein mimics self-assembled from dendritic dipeptides.

Results and Discussion

The structures of the precursor dendritic alcohols (4-3,4-3,5)nG2-CH$_2$OH and the dendritic dipeptides (4-3,4-3,5)nG2-CH$_2$-Boc-L-Tyr-L-Ala-OMe with $n = 1$–16 are shown in Scheme 1.

Preliminary data on the self-assembly of the dendritic dipeptide with $n = 12$ in solution and solid state and on the demonstration that supramolecular structures assembled from the dendritic dipeptides with $n = 6$–16 are porous have been reported (15). The self-assembly of (4-3, 4-3,5)12G2-CH$_2$-Boc-L-Tyr-L-Ala-OMe is schematically illustrated in Fig. 1 (15, 16). Here we present a comparative structural and retrostructural analysis of the supramolecular structures self-assembled from the libraries of achiral dendritic alcohols and dendritic dipeptides, with $n = 1$–16 carried out by a combination of solid-state techniques that involves differential scanning calorimetry (DSC) and small- and wide-angle x-ray diffraction (XRD) experiments performed on powder and oriented fibers. The self-assembly in solution is investigated by a combination of CD and UV spectroscopies.
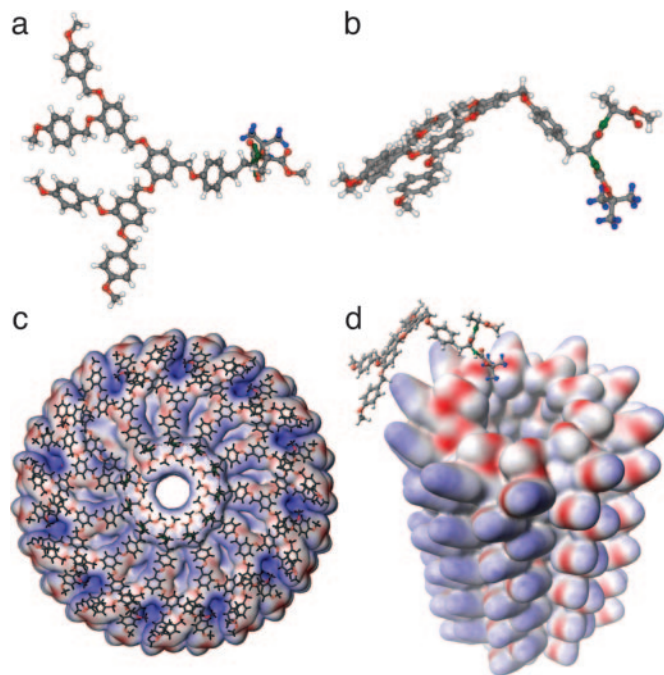
Fig. 1. Self-assembly of (4-3,4-3,5)12G2-CH₂-Boc-L-Tyr-L-Ala-OMe into helical pores. (*a* and *b*) Top (*a*) and side (*b*) views of the dendritic dipeptide. (*c*) Top view of the porous column. (*d*) Tilted view of the pore without dendron. For simplicity all structures are shown with –CH₃ as alkyl groups (15, 16).

Structural Analysis by DSC and Small-Angle XRD. Fig. 2 shows the second heating DSC scans of dendritic alcohols and dendritic dipeptides. All phases were assigned with the aid of temperature-dependent XRD experiments. The first heating and cooling scans and the data collected from all three DSC scans are in
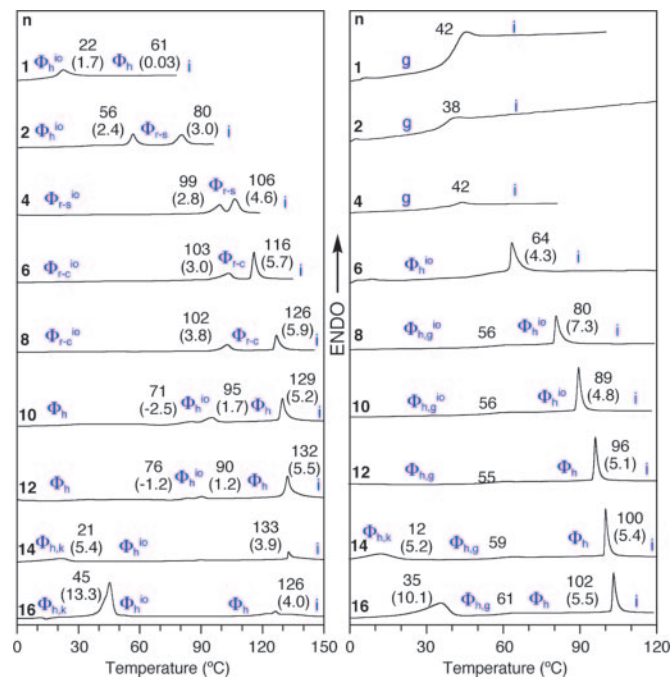

Fig. 2. DSC traces (second heating scans with 10°C per min) of (4-3,4-3,5)nG2-CH₂OH (*Left*) and (4-3,4-3,5)nG2-CH₂-Boc-L-Tyr-L-Ala-OMe (*Right*). Transition temperatures (°C) and enthalpy changes (kcal/mol, in parentheses) are marked by DSC. k, crystal; g, glass; i, isotropic.
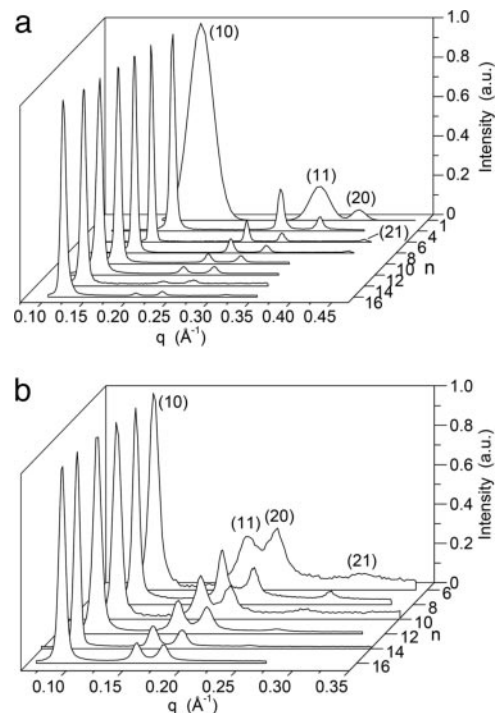

Fig. 3. XRD plots of (4-3,4-3,5)nG2-CH₂OH (*a*) and (4-3, 4-3,5)nG2-CH₂Boc-L-Tyr-L-Ala-OMe (*b*) at 25°C. a.u., arbitrary units.

Table 2 and Figs. 9 and 10, which are published as supporting information on the PNAS web site.

All solid samples are already self-assembled into supramolecular columns that have a circular cross section in the case of various hexagonal columnar lattices (Φ_h) (Φ_h^{io}, $\Phi_{h,g}$, $\Phi_{h,g}^{io}$, and $\Phi_{h,k}$, where g is glassy, k is crystalline, and io is intracolumnar order), or in a slightly distorted ovoidal one in the case of rectangular columnar lattices (Φ_r) [centered rectangular columnar (Φ_{r-c}), simple rectangular columnar (Φ_{r-s}), Φ_{r-c}^{io}, and Φ_{r-s}^{io}]. It is interesting to notice that during the first DSC scan the dendritic alcohols with $n = 4$, 6, and 8 self-assemble into circular columns that self-organize into Φ_h phases. These columns become slightly distorted during subsequent heating and cooling scans and therefore self-organize into Φ_r^{io} phases. During the first heating scan the dendritic dipeptides with $n = 1$, 2, and 4 form Φ_r^{io} phases, whereas during the second scan they produce glassy amorphous solids. Detailed results are in Tables 3 and 4 and Figs. 11 and 12, which are published as supporting information on the PNAS web site.

It is also interesting to notice that the dendritic alcohols with $n = 1$ and 2 provide examples of nonamphiphilic dendrons that self-assemble into supramolecular columns. In all cases the stability of the hexagonal lattices self-organized from dendritic alcohols is ≈52–24°C higher than that of the corresponding dendritic dipeptides. The isotropization temperature of the periodic arrays self-organized from dendritic alcohols increases with n up to $n = 12$ and 14 and subsequently decreases for $n = 16$. In the case of the dendritic dipeptides the isotropization temperature increases continuously as a function of n up to $n = 16$. In addition to the 2D liquid crystalline (Φ_h, Φ_{r-c}, and Φ_{r-s}) and 3D crystalline ($\Phi_{h,k}$) lattices, all alcohols and the dendritic dipeptides with $n = 6$, 8, and 10 self-assemble into structures with long-range io (Φ_h^{io}, Φ_{r-c}^{io}, and Φ_{r-s}^{io}) (17).

Porous supramolecular columns are identified by an increased amplitude of their (11), (20), and (21) diffraction peaks, and the pore diameter (D_{pore}) is calculated by simulating their x-ray diffractogram (15–17). Fig. 3 shows the small-angle XRD for the
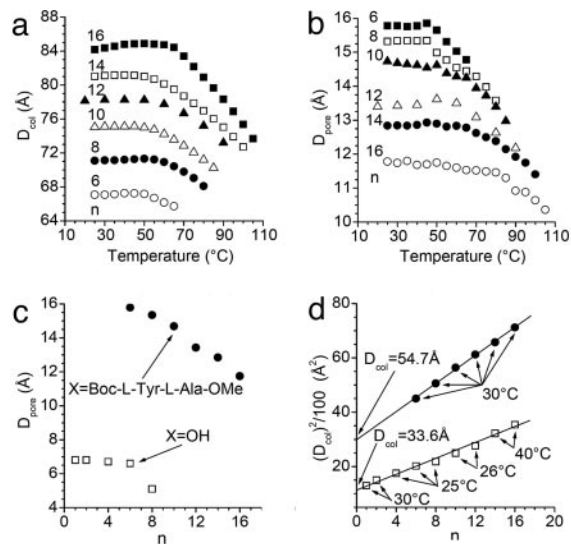
Table 1. Structural and retrostructural analysis of the hexagonal columnar lattices self-organized from (4–3,4–3,5)nG2-CH$_2$-X with X = Boc-L-Tyr-L-Ala-OMe and X = OH, n = 1–16

n	T, °C	$a =$ D_{col},* Å	D_{pore}, Å	ρ_{20}, g/cm^3	μ,[†] dendrons/ column stratum	α',[‡] °
1[§]	20	36.0	6.8	1.23	5.7	63.2
2[§]	30	38.4	6.8	1.12	5.8	62.1
4[§]	90	42.1	6.7	1.12	5.8	62.1
6[§]	90	44.4	6.6	1.12	5.9	61.0
8[§]	60	46.5	5.1	1.10	6.0	60.0
10[§]	26	49.9	<3	1.05	5.9	61.0
12[§]	26	52.6	<3	1.03	6.0	60.0
14[§]	50	56.7	<3	1.03	5.9	61.0
16[§]	65	60.3	<3	1.06	6.5	55.4
6[¶]	30	67.1	15.8	1.12	10.0	36.0
8[¶]	30	71.1	15.3	1.10	10.3	35.0
10[¶]	30	75.1	14.7	1.07	11.2	32.1
12[¶]	25	77.1	13.3	1.02	11.6	31.0
14[¶]	30	81.0	12.7	1.07	11.9	30.3
16[¶]	30	84.4	11.7	1.07	12.8	28.1

*Lattice parameter of Φ_h, $a = 2\langle d_{100}\rangle/3$, $\langle d_{100}\rangle = (d_{100} + \sqrt{3}d_{110} + \sqrt{4}d_{200} + \sqrt{7}d_{210})/4$.

[†]$\mu = (\sqrt{3} \, N_A D^2 \, t\rho)/2M$, $N_A = 6.0220455 \times 10^{23}$ mol^{-1}, height of column stratum $t = 4.7$Å, M = molecular mass of dendron.

[‡]$\alpha' = 2\pi/\mu$ (°).

[§]X = OH.

[¶]X = Boc-L-Tyr-L-Ala-OMe.

Fig. 4. The dependence of D$_{col}$ and D$_{pore}$ of (4-3,4-3,5)nG2-X vs. temperature and n. (a and b) D$_{col}$ (a) and D$_{pore}$ (b) versus temperature x = Box-L-Tyr-L-Ala-OMe. (c) D$_{pore}$ at 30°C. (d) (D$_{col}$)^2 vs. n for x = Boc-L-Tyr-L-Ala-OMe (●) and x = OH (□); the lines show the extrapolation to n = 0.

supramolecular assemblies of the dendritic alcohols and dendritic dipeptides. The first surprise comes from the inspection of the intensities of the XRD of dendritic alcohols (Fig. 3a). The compounds with n = 1–8 show intensities expected for porous supramolecular columns. In the case of both dendritic alcohols and dendritic dipeptides the highest intensities are observed at the lowest values of n. As n increases a continuous decrease of the intensities is observed. The column diameter (D$_{col}$) and D$_{pore}$ were calculated (Table 1) (15–17), and their dependence on temperature is shown in Fig. 4.
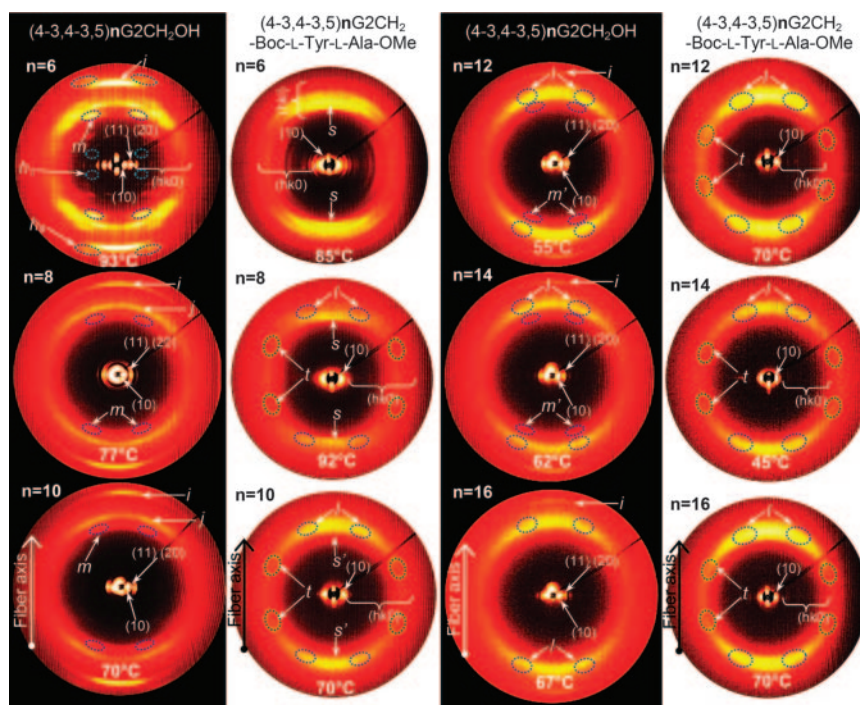
Fig. 5. Wide-angle XRD from oriented fibers of (4-3,4-3,5)nG2-CH$_2$OH (black background) and (4-3,4-3,5)nG2CH$_2$-Boc-L-Tyr-L-Ala-OMe (white background). i, π-π stacking (3.5 ± 0.2 Å); t, tilt feature (60 ± 9°); j, layer thickness in the io phase (4.3 ± 0.2 Å); l, short-range helical feature (4.7 ± 0.2 Å); m, long-range helical feature (5.2 ± 0.2 Å, noted by m' when intensity is weak); (hk), (hk0), and (hkl), reflections of the hexagonal columnar phase; h_1, helical pitch observed for n = 6 (29.3 ± 0.6 Å); h_8, helical feature observed for n = 6; s, sharp feature corresponding to stacking along the column axis (5.2 ± 0.2 Å, noted by s' when intensity is weak).

Percec et al.
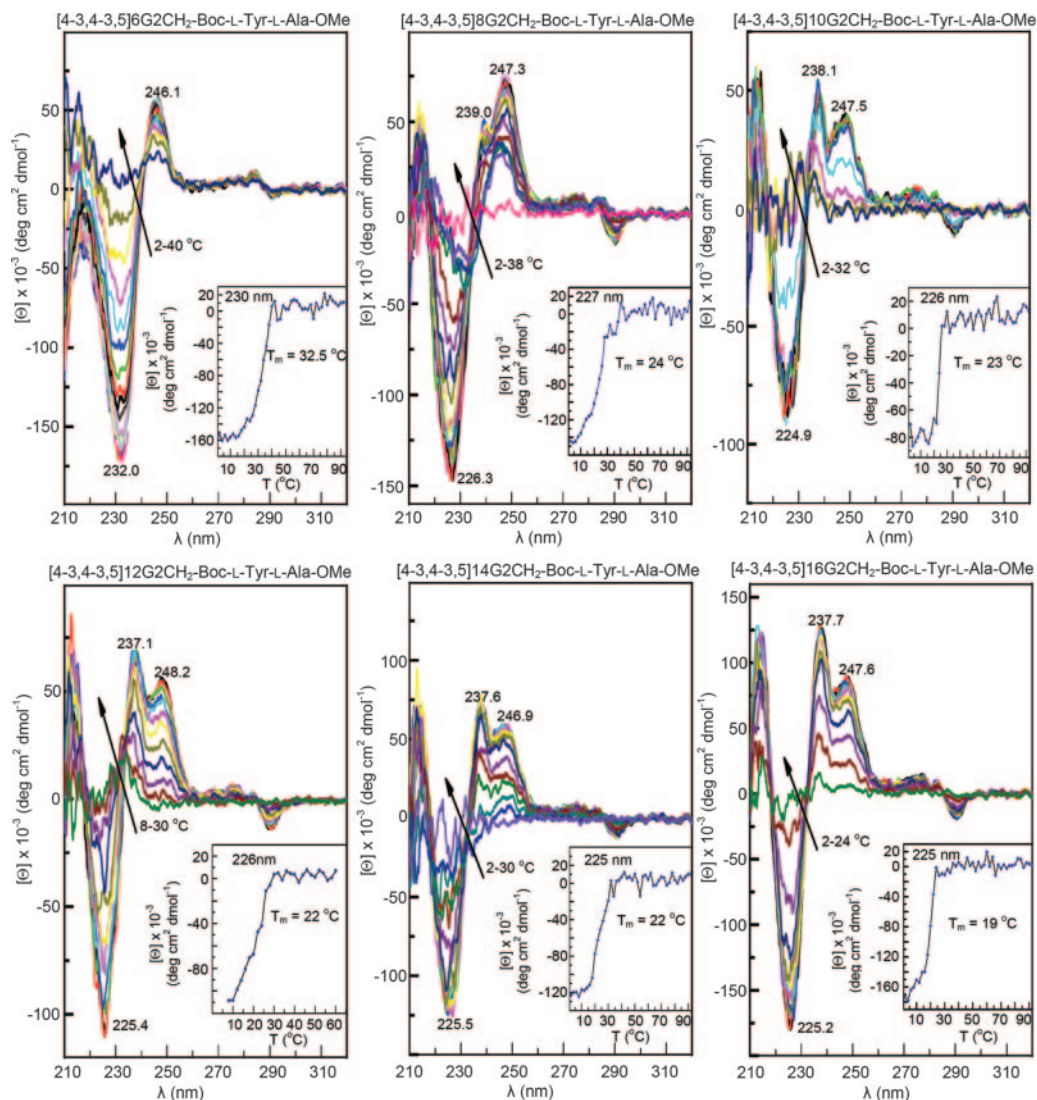
Fig. 6. CD spectra [1.2 × 10⁻⁴ m in methylcyclohexane/cyclohexane 2 per liter (vol/vol)] of (4-3,4-3,5)nG2-CH₂-Boc-L-Tyr-L-Ala-OMe, n = 6, 8, 10, 12, 14, and 16. Arrows indicate trends upon increasing temperature. At higher temperatures only the positive Cotton effect of the dipeptide from 230 nm is observed (Figs. 13 and 14, which are published as supporting information on the PNAS web site). (*Insets*) The dependence of molecular ellipticity on temperature at the wavelength at which the Cotton effect has maximum intensity. The melting temperatures (T_m) of single columns are also indicated.

Previously we have investigated at high temperature the dendritic alcohol with $n = 12$ (15). Within experimental error of our method at high temperature this dendritic alcohol did not assemble into a porous column (15). However, the current study showed that at 25°C the dendritic alcohols with $n = 1$–16 self-assemble into porous columns (Table 1 and Fig. 15, which is published as supporting information on the PNAS web site). The compounds with $n = 10$–16 exhibit D_{pore} at the lower limit of our current calculation method (15–17).

We have reported that in solid state D_{pore} is constant below the glass transition (T_g) and strongly depends on temperature above T_g (16), Here, in agreement with previous results (17), we observe that D_{pore} is constant even above T_g for porous columns with io.

D_{col} and D_{pore} together with the number of dendrons (μ) forming a column stratum and the projection of the solid angle of the dendron (α') (19–22) are summarized in Table 1. For the case of tapered dendrons the solid angle (α) and α' are equal and therefore, for simplicity we will refer to α' as the solid angle. It is both unexpected and remarkable that all dendritic alcohols

self-assemble into porous columns (Table 1 and Fig. 4c). The dependences of $(D_{col})^2$ on n for dendritic alcohols and dendritic dipeptides are shown in Fig. 4d. Their extrapolation to $n = 0$ provides the values of the aromatic parts of the two columns. The difference between these two D_{col} at $n = 0$ gives the diameter of the inner part of the column that contains the dipeptide pore.

Structural Analysis of Oriented Fibers by XRD and Self-Assembly in Solution by CD. Fig. 5 shows the combined small- and wide-angle XRD obtained from oriented fibers of dendritic alcohols and dendritic dipeptides with $n = 6$–16. The assignment of these diffractions is shown in Fig. 5. As observed from the DSC data in Fig. 2 all structures assembled from dendritic alcohols display a higher io than their corresponding supramolecular dendritic dipeptides. The dendritic dipeptides exhibit the highest io for $n = 6$ and 8 followed by $n = 10$. All supramolecular columns self-assembled from achiral dendritic alcohols and chiral dendritic dipeptides are helical. The helicity of the columns self-assembled from achiral dendritic alcohols provides definitive demonstration for our previous hypothesis that the helicity of the

Fig. 7. Supramolecular helical column self-assembled from (4-3,4-3,5)6G2-CH$_2$OH. (*a*) Side view of the central region of the column with H bonds indicated by dotted lines (alkyl group is not shown). For one of the aromatic rings a surface was added to indicate helical parking. (*b*) Space-filling surface of the same structure. (*c*) Wide-angle fiber XRD (fiber axis is horizontal) obtained at 93°C showing the io structure, helical pitch $h_1 \approx 29$ Å, h_{1-8}, long-range helical features, π-π stacking, and the first four diffractions of the Φ_h (in expanded area). The models in *a* and *b* were constructed by molecular modeling of the XRD from *c* together with experimental density.

dendritic dipeptides is induced by their achiral dendrons (15, 16). This self-assembly system relates to other processes in which a stereocenter selects the twist sense of a racemic helical structure (10, 23, 24) and is in agreement with the principles elaborated by Green *et al.* (25). However, it differs from those in which a stereocenter induces helicity in an achiral nonhelical system (26). Other examples of helical supramolecular dendrimers self-assembled from achiral dendrons are known (27, 28). Therefore, as previously assumed, the stereochemistry of the dipeptide selects only the handedness of an already helical structure (15, 16). The self-assembly of dendritic dipeptides with $n = 6$–16 was monitored in a solvophobic mixture of solvents by CD (Fig. 6) and UV (Figs. 13 and 14) spectroscopies (15, 16). The molecular solution of the dendritic dipeptide shows a positive Cotton effect at 230 nm (Figs. 13 and 14). On cooling, self-assembly takes place and several positive and negative Cotton effects that were assigned to the aromatic part of the dendron (15, 16) appear. Two important events must be followed in Fig. 6: first, the general trend of the ellipticity and the sign of the Cotton effects, and second, the melting temperature of the single column in solution. Particularly interesting is that the sign of the Cotton effects from 210 and 237 nm changes from negative in $n = 6$ to positive in all other n. In $n = 6$ the Cotton effects at 225 and 237

nm are both negative and give an overlapped Cotton effect centered at 231 nm. As n increases the Cotton effect at $\approx$237 nm becomes positive and its ellipticity increases. Although the CD of the self-assembled structure is not yet completely assigned, it demonstrates that variation of n induces changes in the intramolecular and supramolecular conformation of the aromatic part of the dendron. Melting temperature of the single supramolecular structure also depends on n and varies from 32.5°C for $n = 6$ to 19°C for $n = 16$. Therefore, the dendritic dipeptide with $n = 6$ is more suitable for single-channel experiments performed in phospholipid vesicles than the dipeptide with $n = 12$ that was used previously (15).

Principles of Helical Pore Assembly. Fig. 7 shows the helical porous structure self-assembled from (4-3,4-3,5)6G2-CH$_2$OH. The models of the top view of the single column strata self-assembled from (4-3,4-3,5)6G2-CH$_2$OH and (4-3,4-3,5)6G2-CH$_2$-Boc-L-Tyr-L-Ala-OMe are shown in Fig. 8 (Table 1). The difference between D$_{col}$ of the column self-assembled from the dendritic dipeptide and dendritic alcohol, both at $n = 0$, is $\approx$20 Å (Table 1 and Fig. 3*d*). This value represents the difference between the inner parts of the two columns that include the dipeptide and the pore. About 10 Å from this difference is caused by the thickness of the dipeptide (Fig. 8 *Upper Right*) that is 5 Å $\times$ 2 = 10 Å. The rest comes from the difference between the D$_{pore}$ of the dendritic dipeptide column and the dendritic alcohol column. For $n = 6$ this difference is $\approx$10 Å (Table 1). The agreement between model and experimental data demonstrates that the structural model of the porous column is correct and suggests molecular strategies for pore design.

An inspection of Fig. 8 and Table 1 provides access to the fundamental principles of pore assembly from dendritic dipeptides. At the transition from dendritic alcohol to dendritic dipeptide the number of dendrons forming a column stratum (μ) increases from 5.9 to 10, and subsequently D$_{pore}$ increases from 6.6 to 15.8 Å. Attaching the dipeptide to the apex of the dendritic alcohol decreases α' from 61° to 36° (Fig. 8). This process is equivalent with the synthesis of a new dendron that has a primary structure that provides a smaller α' (18). This concept is also in agreement with the change of α' via different protecting groups attached to the dipeptide (17). In all these cases a decrease in α' increases μ, and this sequence increases the pore size of the column. However, the influence of μ within a homologous series of dendritic alcohols and dendritic dipeptides has the reversed effect (Table 1). When α' decreases, D$_{pore}$ decreases in the series of supramolecular structures designed from both dendritic alcohols and dendritic dipeptides. A quantitative explanation of this unexpected and complex trend requires knowledge on the

Fig. 8. Principles of helical pore assembly from dendritic dipeptides. (*Left*) Models of supramolecular column strata self-assembled from (4-3,4-3,5)6G2-CH$_2$OH and (4-3,4-3,5)6G2-CH$_2$-Boc-L-Tyr-L-Ala-OMe. All models were constructed by molecular modeling of the XRD data together with experimental density. (*Right*) The supramolecular pore assembled from (4-3,4-3,5)6G2-Boc-L-Tyr-1-Ala-OMe. Only its dipeptide part is shown.

fractions of trans and gauche conformers of the methylenic units of the dendron as a function of *n*.

Conclusions

The results reported here and in previous publications (15–18) demonstrate a complex mechanism for the self-assembly of supramolecular porous structures from dendritic dipeptides. This mechanism involves cooperativity (15) and allosteric regulation (16). However, the currently generated data already provide the molecular principles required to address the molecular design of supramolecular helical porous structures with diameter controlled at the Å level from a single dendritic dipeptide primary structure via a combination of architectural motifs that involve dipeptide stereochemistry (15, 16), protective groups (17), and the number of methylenic units (*n*) from the periphery of the dendron. These results also provide strategies for the design of helical porous assemblies by the self-assembly of dendrons that contain other functional groups in addition to dipeptides at their apex. These design principles apply most

probably to libraries of dendritic dipeptides containing multiple dendrons and dipeptides with various primary structures. We expect that these design principles will expand the scope and limitations of biologically inspired functions (15) created from porous protein mimics self-assembled from dendritic dipeptides and broaden the synthetic capabilities of dendrimers and dendrons (29).

Materials and Methods

The synthesis of (4-3,4-3,5)nG2-CH$_2$OH and (4-3,4-3,5)nG2-CH$_2$-Boc-L-Tyr-L-Ala-OMe with *n* = 1–16 was carried out as described (15). The structural and retrostructural analysis methods used in these investigations were developed in our laboratory (15) and are elaborated in *Supporting Text*, which is published as supporting information on the PNAS web site, and Tables 3 and 4.

1. Klug, A. (1983) *Angew. Chem. Int. Ed.* **22,** 565–582.
2. MacKinnon, R. (2004) *Angew. Chem. Int. Ed.* **43,** 4265–4277.
3. Agre, P. (2004) *Angew. Chem. Int. Ed.* **43,** 4278–4290.
4. Wallace, B. A. (1986) *Biophys. J.* **49,** 295–306.
5. Gouaux, E. (1998) *J. Struct. Biol.* **121,** 110–122.
6. Ishii, D., Kinbara, K., Ishida, Y., Ishii, N., Okochi, M., Yohda, M. & Aida, T. (2003) *Nature* **423,** 628–632.
7. Bayley, H. & Cremer, P. S. (2001) *Nature* **413,** 226–230.
8. Ghadiri, M. R., Granja, J. R., Milligan, R. A., McRee, D. E. & Khazanovich, N. (1993) *Nature* **366,** 324–327.
9. Petitjean, A., Cuccia, L. A., Lehn, J.-M., Nierengarten, H. & Schmutz, M. (2002) *Angew. Chem. Int. Ed.* **41,** 1195–1198.
10. Hill, D. J., Mio, M. J., Prince, R. B., Hughes, T. S. & Moore, J. S. (2001) *Chem. Rev.* **101,** 3893–4012.
11. Nolte, R. J. M., van Beijnen, A. J. M., Neevel, J. G., Zwikker, J. W., Verkley, A. J. & Drenth, W. (1984) *Isr. J. Chem.* **24,** 297–301.
12. Bong, D. T., Clark, T. D., Granja, J. R. & Ghadiri, M. R. (2001) *Angew. Chem. Int. Ed.* **40,** 988–1011.
13. Sakai, N., Mareda, J. & Matile, S. (2005) *Acc. Chem. Res.* **38,** 79–87.
14. Fenniri, H., Deng, B.-L. & Ribbe, A. E. (2002) *J. Am. Chem. Soc.* **124,** 11064–11072.
15. Percec, V., Dulcey, A. E., Balagurusamy, V. S. K., Miura, Y., Smidrkal, J., Peterca, M., Nummelin, S., Edlund, U., Hudson, S. D., Heiney, P. A., *et al.* (2004) *Nature* **430,** 764–768.
16. Percec, V., Dulcey, A. E., Peterca, M., Ilies, M., Ladislaw, J., Rosen, B. M., Edlund, U. & Heiney, P. A. (2005) *Angew. Chem. Int. Ed.* **44,** 6516–6521.
17. Percec, V., Dulcey, A. E., Peterca, M., Ilies, M., Sienkowska, M. J. & Heiney, P. A. (2005) *J. Am. Chem. Soc.* **127,** 17902–17909.
18. Percec, V., Dulcey, A. E., Peterca, M., Ilies, M., Miura, Y., Edlund, U. & Heiney, P. A. (2005) *Aust. J. Chem.* **58,** 472–482.
19. Ungar, G., Percec, V., Holerca, M. N., Johansson, G. & Heck, J. A. (2000) *Chem. Eur. J.* **6,** 1258–1266.
20. Percec, V., Cho, W.-D. & Ungar, G. (2000) *J. Am. Chem. Soc.* **122,** 10273–10281.
21. Percec, V., Cho, W.-D., Ungar, G. & Yeardley, D. J. P. (2001) *J. Am. Chem. Soc.* **123,** 1302–1315.
22. Percec, V., Mitchell, C. M., Cho, W.-D., Uchida, S., Glodde, M., Ungar, G., Zeng, X., Liu, Y., Balagurusamy, V. S. K. & Heiney, P. A. (2004) *J. Am. Chem. Soc.* **126,** 6078–6094.
23. Brunsveld, L., Zhang, H., Glasbeek, M., Vekemans, J. A. J. M. & Meijer, E. W. (2000) *J. Am. Chem. Soc.* **122,** 6175–6182.
24. Jin, W., Fukushima, T., Niki, M., Kosaka, A., Ishii, N. & Aida, T. (2005) *Proc. Natl. Acad. Sci. USA* **102,** 10801–10806.
25. Green, M. M., Park, J.-W., Sato, T., Teramoto, A., Lifson, S., Selinger, R. L. B. & Selinger, J. V. (1999) *Angew. Chem. Int. Ed.* **38,** 3139–3154.
26. Engelkamp, H., Middelbeek, S. & Nolte, R. J. M. (1999) *Science* **284,** 785–788.
27. Percec, V., Glodde, M., Bera, T. K., Miura, Y., Shiyanovskaya, I., Singer, K. D., Balagurusamy, V. S. K., Heiney, P. A., Schnell, I., Rapp, A., *et al.* (2002) *Nature* **419,** 384–387.
28. Percec, V., Ahn, C.-H., Ungar, G., Yeardley, D. J. P., Möller, M. & Sheiko, S. S. (1998) *Nature* **391,** 161–164.
29. Emrick, T. & Fréchet, J. M. J. (1999) *Curr. Opin. Colloid Interface Sci.* **4,** 15–23.

CHEMISTRY